REPORT DOCUMENTATION PAGE

The public reporting burden for this collection of information is estimated to average 1 hour per response, including the time for reviewing instructions, searching existing data sources, gathering and maintaining the data needed, and completing and reviewing the collection of information. Send comments regarding this burden estimate or any other aspect of this collection of information, including suggestions for reducing the burden, to the Department of Defense, Executive Services and Communications Directorate (0704-0188). Respondents should be aware that notwithstanding any other provision of law, no person shall be subject to any penalty for failing to comply with a collection of information if it does not display a currently valid OMB control number.
PLEASE DO NOT RETURN YOUR FORM TO THE ABOVE ORGANIZATION.

1. REPORT DATE *(DD-MM-YYYY)*	2. REPORT TYPE	3. DATES COVERED *(From - To)*
05-08-2009	Journal Article	

4. TITLE AND SUBTITLE	5a. CONTRACT NUMBER
Impact of GODAE Products on Nested HYCOM Simulations of the West Florida Shelf	
	5b. GRANT NUMBER
	5c. PROGRAM ELEMENT NUMBER
	0601153N

6. AUTHOR(S)	5d. PROJECT NUMBER
G. Halliwell, A. Barth, Robert Weisberg, Patrick J. Hogan, Ole Martin Smedstad, James A. Cummings	
	5e. TASK NUMBER
	5f. WORK UNIT NUMBER
	73-8554-08-5

7. PERFORMING ORGANIZATION NAME(S) AND ADDRESS(ES)	8. PERFORMING ORGANIZATION REPORT NUMBER
Naval Research Laboratory Oceanography Division Stennis Space Center, MS 39529-5004	NRL/JA/7320-08-8095

9. SPONSORING/MONITORING AGENCY NAME(S) AND ADDRESS(ES)	10. SPONSOR/MONITOR'S ACRONYM(S)
Office of Naval Research 800 N. Quincy St. Arlington, VA 22217-5660	ONR
	11. SPONSOR/MONITOR'S REPORT NUMBER(S)

12. DISTRIBUTION/AVAILABILITY STATEMENT

Approved for public release, distribution is unlimited.

20090814045

13. SUPPLEMENTARY NOTES

14. ABSTRACT

Nested non-assimilative simulations of the West Florida Shelf for 2004 -2005 are used to quantify the impact of initial and boundary conditions provided by Global Ocean Data Assimilation Experiment ocean products. Simulations are nested within an optimum interpolation hindcast of the Atlantic Ocean, the initial test of the US Navy Coupled Ocean Data Assimilation system for the Gulf of Mexico, and a global ocean hindcast that used the latter assimilation system. These simulations are compared to one that is nested in a non-assimilative Gulf of Mexico model to document the importance of assimilation in the outer model. Simulations are evaluated by comparing model results to moored Acoustic Doppler Current Profiler measurements and moored sea surface temperature time series. The choice of outer model has little influence on simulated velocity fluctuations over the inner and middle shelf where fluctuations are dominated by the deterministic wind-driven response. Improvement is documented in the representation of alongshore flow variability over the outer shelf, driven in part by the intrusion of the Loop Current and associated cyclones at the shelf edge near the Dry Tortugas. For temperature, the non-assimilative outer model had a cold bias in the upper ocean that was substantially corrected in the data-assimilative outer models, leading to improved temperature representation in the simulations nested in the assimilative outer models.

15. SUBJECT TERMS

numerical modeling, coastal circulation

16. SECURITY CLASSIFICATION OF:			17. LIMITATION OF ABSTRACT	18. NUMBER OF PAGES	19a. NAME OF RESPONSIBLE PERSON
a. REPORT	b. ABSTRACT	c. THIS PAGE			Patrick Hogan
Unclassified	Unclassified	Unclassified	UL	17	19b. TELEPHONE NUMBER *(Include area code)* 228-688-4537

Impact of GODAE products on nested HYCOM simulations of the West Florida Shelf

George R. Halliwell Jr · Alexander Barth ·
Robert H. Weisberg · Patrick Hogan ·
Ole Martin Smedstad · James Cummings

Abstract Nested non-assimilative simulations of the West
Florida Shelf for 2004–2005 are used to quantify the impact
of initial and boundary conditions provided by Global
Ocean Data Assimilation Experiment ocean products.
Simulations are nested within an optimum interpolation
hindcast of the Atlantic Ocean, the initial test of the US
Navy Coupled Ocean Data Assimilation system for the
Gulf of Mexico, and a global ocean hindcast that used the
latter assimilation system. These simulations are compared
to one that is nested in a non-assimilative Gulf of Mexico
model to document the importance of assimilation in the
outer model. Simulations are evaluated by comparing
model results to moored Acoustic Doppler Current Profiler
measurements and moored sea surface temperature time
series. The choice of outer model has little influence on
simulated velocity fluctuations over the inner and middle
shelf where fluctuations are dominated by the deterministic
wind-driven response. Improvement is documented in the
representation of alongshore flow variability over the outer
shelf, driven in part by the intrusion of the Loop Current
and associated cyclones at the shelf edge near the Dry
Tortugas. This improvement was realized in the simulation
nested in the global ocean hindcast, the only outer model
choice that contained a realistic representation of Loop
Current transport associated with basin-scale wind-driven
gyre circulation and the Atlantic Meridional Overturning
Circulation. For temperature, the non-assimilative outer
model had a cold bias in the upper ocean that was
substantially corrected in the data-assimilative outer mod-
els, leading to improved temperature representation in the
simulations nested in the assimilative outer models.

Responsible editor: Pierre De Mey

G. R. Halliwell Jr (✉)
MPO/RSMAS, University of Miami,
4600 Rickenhacker Causeway,
Miami, FL, USA
e-mail: ghalliwell@rsmas.miami.edu

A. Barth
GHER/AGO, University of Liege,
Liege, Belgium

R. H. Weisberg
University of South Florida,
St. Petersburg, FL, USA

P. Hogan
Naval Research Laboratory,
Stennis Space Center, MS, USA

O. M. Smedstad
QinetiQ North America, Technology Solutions Group, PSI,
Stennis Space Center, MS, USA

J. Cummings
Naval Research Laboratory,
Monterey, CA, USA

1 Introduction

At the open boundaries of coastal ocean models, it is
necessary to prescribe an accurate representation of
momentum and water properties along with their cross-
boundary fluxes. This is required to properly represent the
influence of offshore processes such as boundary current
and eddy variability on coastal ocean circulation. Regional
to global ocean hindcasts generated as part of the Global
Ocean Data Assimilation Experiment (GODAE) are an
attractive choice for providing this offshore forcing.

Nesting coastal models is desirable because GODAE products are suboptimal for studying the coastal ocean due to factors such as insufficient horizontal, vertical, and temporal resolution in model output, the use of low-resolution atmospheric forcing, inadequate representation of river/estuarine runoff, and the absence of tidal forcing. Since GODAE products are now in various stages of development and evaluation, their strengths and weaknesses for providing initial fields and offshore boundary forcing to nested coastal models remain to be evaluated.

In addition to energetic forcing by the atmosphere and coastal river/estuarine runoff, the West Florida Shelf (WFS, Fig. 1) is influenced by energetic offshore variability associated with the Loop Current (LC) and adjacent rings and eddies. These offshore features influence property exchanges across the shelfbreak, and the LC can, under certain conditions, exert a strong influence on the flow and thermodynamical structure over the shelf (Paluszkiewicz et al. 1983; He and Weisberg 2003; Weisberg and He 2003). Because of the Taylor–Proudman constraint stating that low Rossby number currents will flow parallel to local isobaths if friction and time dependence are negligible, the direct dynamical influence of offshore eddy forcing over a continental shelf much wider than the local Rossby radius of deformation will remain confined to the outer shelf (e.g., Chapman and Brink 1987; Kelly and Chapman 1988). This scenario is true along most of the WFS except at the northern end near the DeSoto Canyon and at the southwestern end near the Dry Tortugas (Fig. 1). The narrow shelf near DeSoto Canyon permits eddy fluctuations to strongly impact shelf circulation and produce large cross-shelf exchanges (Huh et al. 1981; Weisberg et al. 2004, 2005). The LC influences outer shelf flow along the entire WFS when its path is situated adjacent to the shelfbreak near the Dry Tortugas (e.g., Hetland et al. 1999). Pressure perturbations over the shelf induced by LC flow in this region propagate northward, and the resulting geostrophic adjustment produces southward flow over the entire shelf (Weisberg and He 2003). In contrast, a LC intrusion event along the broad central WFS was confined to the outer shelf due to the Taylor–Proudman constraint (He and Weisberg 2003). When the Taylor–Proudman constraint is broken, either by pressure perturbation adjustment across shallow isobaths or directly by bottom friction, a significant cross-shelf transport of offshore water may occur within the bottom boundary layer (He and Weisberg 2003; Weisberg and He 2003; Weisberg et al. 2004).

This offshore influence coexists with large variability driven by synoptic atmospheric systems, particularly tropical waves and cyclones in summer/fall, and cold front passages during the remainder of the year (Niiler 1976; Mitchum and Sturges 1982; Cragg et al. 1983; Marmorino 1983; Mitchum and Clarke 1986a,b; Weisberg et al. 2001).
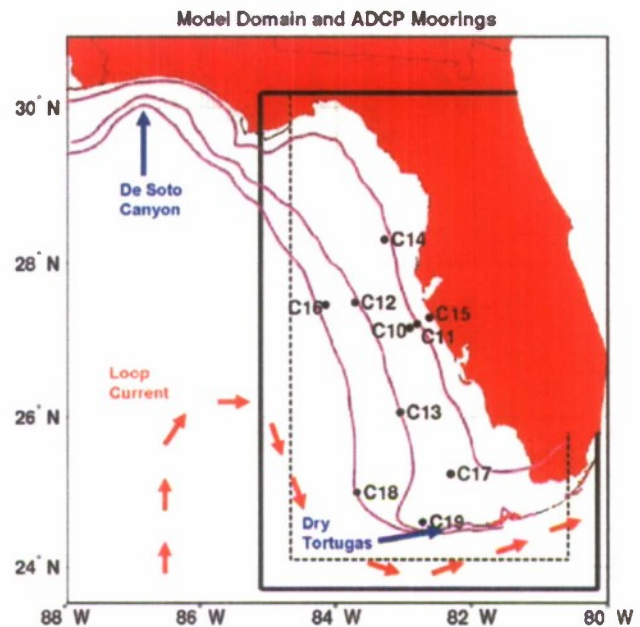

Fig. 1 Locations of the West Florida Shelf COMPS ADCP Moorings C10 to C19 along with the boundaries of the nested model domain. *Dashed lines* outline the nesting relaxation boundary zones. The 20-, 50-, and 100-m isobaths are shown as a schematic of the Loop Current path

The inner shelf responds to wind through a classical Ekman-geostrophic spinup (Weisberg et al. 2000), while stratification is very influential in that it (1) sets the vertical distribution of mixing and hence the Ekman layer interactions and (2) produces an upwelling and downwelling response asymmetry by thermal wind effects on the bottom Ekman layer (Weisberg et al. 2001). As a result, wind-driven downwelling currents tend to be confined closer to the coast than upwelling currents (Liu and Weisberg 2005, 2007). This atmospherically forced response is not totally independent of the response to offshore forcing. Large time-dependent variability between upwelling- and downwelling-favorable winds along with large friction present in both the surface and bottom boundary layers can break the Taylor–Proudman constraint and permit large cross-shelf transport of water properties (Weisberg et al. 2005).

The two scientific goals of this paper are to (1) evaluate the impact of GODAE ocean hindcasts on simulations of the WFS and (2) evaluate a regional implementation of the Hybrid Coordinate Ocean Model (HYCOM) as part of a larger effort to develop an ocean model with a sufficiently flexible vertical coordinate to quasi-optimally represent the transition between the deep and coastal ocean. The first goal addresses the central theme of this special issue and also addresses a specific GODAE objective: apply state-of-the-art models and assimilation methods to produce boundary conditions that extend predictability of coastal and regional subsystems (International GODAE Steering Team 2000).

To address these goals, three GODAE data-assimilative ocean hindcasts are evaluated for providing offshore forcing to nested WFS simulations. These hindcasts all use the HYCOM and represent different stages of the ongoing development of the next-generation US Navy ocean nowcast–forecast system. Due to ongoing improvements in model physics and parameterizations, resolution, bathymetry, and assimilation techniques, significant differences exist in the representation of the offshore ocean among these HYCOM-based products. This fact enables meaningful sensitivity studies to be conducted by nesting non-assimilative WFS simulations within them. The impact of nesting within data-assimilative outer models is also contrasted against nesting within a non-assimilative ocean model. This comparison is designed to identify improvements in the nested coastal simulation that are achieved when the outer model more realistically represents offshore currents and eddies. Barth et al. (2008) nested WFS simulations performed with the Regional Ocean Modeling System (ROMS) in climatology and in a HYCOM-based data-assimilative ocean hindcast and documented improvements in the flow field produced by the model nested in the ocean hindcast.

This paper is organized as follows: The ocean model is described in Section 2, the GODAE ocean products used to provide initial and boundary conditions are described in Section 3, and the moored observations against which the nested ocean simulations are evaluated are described in Section 4. The setup of the nested WFS simulations along with evaluation procedures are outlined in Section 5. Section 6 documents the sensitivity of simulated velocity fluctuations over the WFS to the different outer model products, while Section 7 documents the sensitivity of simulated surface temperature fluctuations. Conclusions are presented in Section 8. The study of Kourafalou et al. (2008) complements the present analysis by focusing on the impact of GODAE products in the South Florida coastal region, including the Florida Straits.

2 Model description

The HYCOM (http://www.hycom.org) is designed to use Lagrangian isopycnic coordinates throughout as much of the stratified ocean interior as possible but perform a dynamical transition to fixed vertical coordinates, either level (p) or terrain-following (σ), in regions where isopycnic coordinates are suboptimum. Fundamental properties of the model are presented in Bleck (2002), Chassignet et al. (2003), and Halliwell (2004). Since basic features of the model are also summarized in Kourafalou et al. (2008), the present discussion is limited to model features central to this study.

HYCOM evolved from the Miami Isopycnic-Coordinate Model (MICOM; Bleck et al. 1992; Bleck 1998), Although fixed coordinates are maintained in some regions, the model remains a purely Lagrangian layer model, and the procedures used to solve MICOM equations are unmodified except for executing the hybrid "grid generator" at the end of each baroclinic time step to relocate layer interfaces (Bleck 2002). HYCOM therefore remains a Lagrangian vertical dynamics (LVD) model where the continuity (thickness tendency) equation is solved prognostically throughout the domain. Fixed p or σ coordinates are maintained by the grid generator, which is essentially an arbitrary Lagrangian–Eulerian (ALE) technique (e.g., Adcroft and Hallberg 2005) that re-maps the vertical coordinates back to their fixed positions after each time step. The model maintains smooth, thin transition zones between the Lagrangian and fixed coordinate domains.

One advantage of the LVD model is that level p coordinates can be used in regions of sloping topography without the numerical difficulties encountered by z coordinate models such as the Modular Ocean Model (MOM). MOM is an Eulerian vertical dynamics (EVD) model that uses the continuity equation to diagnose vertical velocity, and numerical difficulties in representing the step-like structure of the sloping bottom must be reduced by employing special numerical techniques (e.g., Adcroft et al. 1997). Instead, HYCOM handles the intersection of level p coordinates with the bottom (where layers collapse to zero thickness) in exactly the same manner as for isopycnic coordinates. Given that either p or σ coordinates can be used in shallow water regions, special tests were conducted to determine that level p coordinates are the optimum choice (Appendix). For this study, p coordinates are used over the continental shelf except within the 10 m isobath where the upper three layers are permitted to deform to σ coordinates to maintain vertical resolution all the way to the coast (the 2-m isobath).

The model contains several vertical mixing choices (Halliwell 2004), with the K-profile parameterization (KPP; Large et al. 1994) being used in the present study. The original KPP mixing model evaluated by Halliwell (2004) did not contain an explicit parameterization of the bottom boundary layer, but one has since been added. The procedure is the same as for the surface boundary layer, first diagnosing the turbulent boundary layer thickness and then estimating K profiles for momentum and scalars at model interfaces that smoothly match the interior profiles above. In regions where the surface and bottom boundary layers overlap, the largest K values are chosen at each interface. At the bottom, of course, there are no normal mass fluxes, while the only heat fluxes are provided by penetrating shortwave radiation that heats the bottom surface, a negligible effect except in very shallow water.

Bottom friction velocity u_b* is the dominant parameter governing the diagnosed bottom boundary layer thickness and thus the magnitude of the diagnosed K values, which are linearly proportional to this thickness.

3 Data assimilative GODAE products

Products from the evolving ocean nowcast–forecast system under development by the US Navy (e.g., Chassignet et al. 2006, 2007) provide the initial and boundary fields in which the coastal simulations are nested. The initial incarnation of this system (ATL-OI) was run in the Atlantic basin at a resolution of 0.08°. It employed optimum interpolation (OI) to assimilate sea surface height anomaly (SSHA) from satellite altimetry, with the Cooper and Haines (1996) technique providing downward projection of information to constrain temperature and salinity profiles. Specifically, the two-dimensional Modular Ocean Data Assimilation System (MODAS) 0.25° SSHA analysis (Jacobs et al. 2001; Fox et al. 2002) is assimilated daily. To generate these SSHA maps, real-time satellite altimeter data [GEOSAT-Follow-On (GFO), ENVISAT, and Jason-1] are analyzed at the Altimeter Data Fusion Center at NAVOCEANO. In addition to SSHA, SST is assimilated by relaxing model fields to the daily MODAS 0.125° SST analysis, which uses the daily Multi-Channel Sea Surface Temperature product derived from Advanced Very High Resolution Radiometer data.

The two other hindcast products evaluated herein both use the Navy Coupled Ocean Data Assimilation (NCODA) system. NCODA is an oceanographic version of the multivariate optimum interpolation (Cummings 2005) technique widely used in operational atmospheric forecasting systems. The NCODA system assimilates satellite altimetry track-by-track and SST directly from orbital data using model forecasts as the first guess. The system assimilates more data types than the previous OI system. However, since the availability of in situ observations is generally very limited in the open gulf (e.g., ARGO floats are usually not present), the NCODA assimilation in this region still relies primarily on satellite altimetry and SST measurements. As for the OI system, the Cooper and Haines (1996) algorithm is used to constrain temperature and salinity profiles. In both the NCODA and OI systems, the impact of altimetry assimilation is tapered to zero toward the coast between the middle and upper regions of the continental slope. This tapering does not degrade the representation of the LC along with its associated warm rings and cold eddies since, these features are sufficiently far offshore to be fully constrained by the data assimilation. In all assimilation systems, the model runs free in the absence of observations.

The two incarnations of the NCODA system evaluated herein were run in the Gulf of Mexico (GoM-NCODA) and globally (GLB-NCODA). The regional GoM-NCODA represents the initial test of the NCODA system and was run at a resolution of 0.04°. The non-assimilative (GoM-free) simulation that is also evaluated herein was run in the identical domain. Both GoM-NCODA and GoM-free were nested in a climatology generated from a multi-year, climatologically forced, 0.08° HYCOM Atlantic Ocean simulation. Kourafalou ct al. (2008) provides additional information on both of these products. For all data-assimilative hindcasts used herein, the assimilation tends to situate the LC along with adjacent rings and eddies in the correct location (Chassignet et al. 2005; Halliwell et al. 2008). However, the climatological boundary conditions used for GoM-NCODA ensure that LC transport variability associated with the basin-scale wind-driven gyres and with the Atlantic Meridional Overturning Circulation is incorrectly represented. In contrast, GLB-NCODA produces LC transport fluctuations that more accurately represent variability associated with the offshore gyre and overturning variability. Comparison between the simulations nested in GoM-NCODA and GLB-NCODA therefore highlights the impact of these transport differences on the nested models.

4 Observations

The University of South Florida has implemented a real-time Coastal Ocean Monitoring and Prediction System (COMPS; http://comps.marine.usf.edu) for the WFS. COMPS consists of an array of instrumentation both along the coast and offshore, combined with numerical circulation models, and builds upon existing in situ measurements and modeling programs funded by various state and federal agencies. An array of offshore buoys measure current, temperature, salinity, and meteorological parameters, with satellite telemetry of the data to the shore. For the present study along with the South Florida study of Kourafalou et al. (2008), velocity profile observations are obtained from nine ADCP moorings C10 through C19 (Fig. 1), while sea surface temperature is obtained from several of them. Tidal variability (He and Weisberg 2002) was removed from these records prior to analysis since tidal forcing was not present in the model simulations. Velocity measurements are recorded hourly at depth intervals of 1 m, with data availability as a function of depth and time summarized in Fig. 2. To obtain the longest possible time series, short gaps evident in Fig. 2, along with some very short gaps of 1 or 2 h that are not visually evident in Fig. 2, were filled using either linear interpolation in time or downward extrapolation in depth for those cases where near-bottom measurements dropped out. Hourly surface temperature measurements are also obtained from several of these mooring.
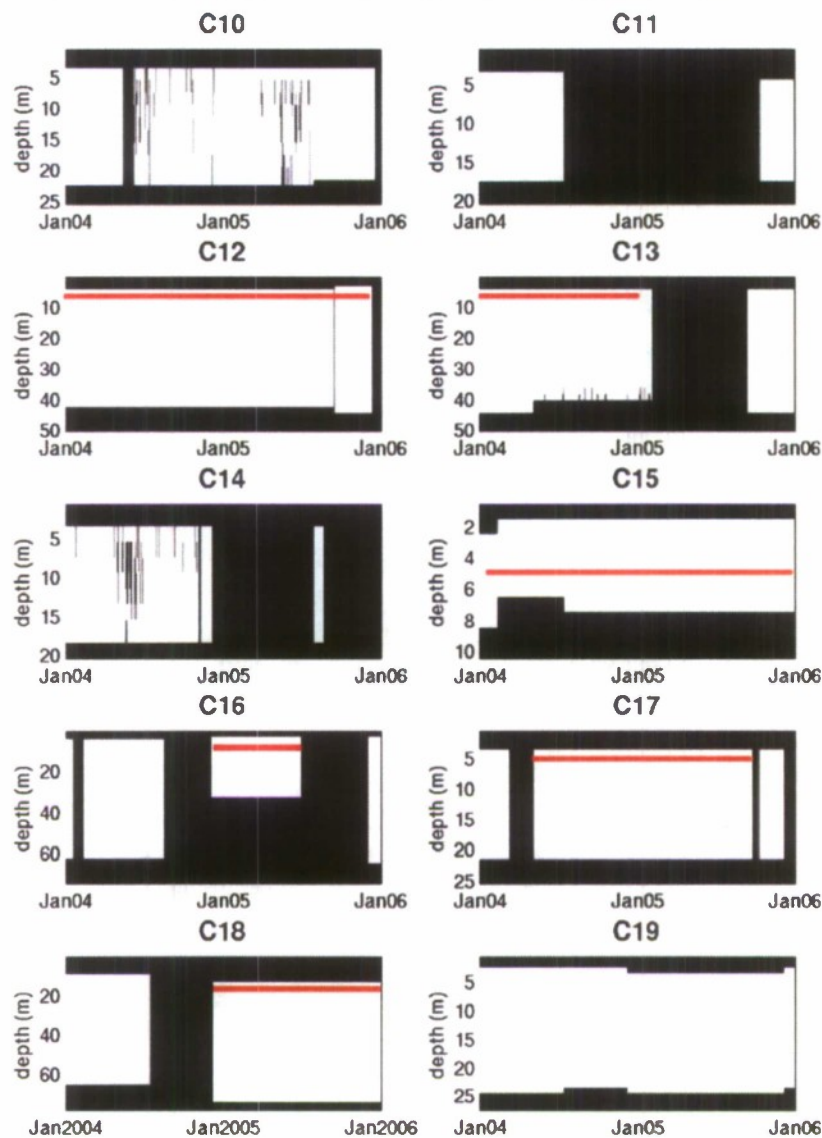
Fig. 2 Depth–time plot of ADCP data availability at the nine COMPS ADCP moorings in Fig. 1. Depths and times with missing data are blacked out. Very short 1–2-h gaps present at some moorings are not visible. The *horizontal red bars* show the depth and time range of the velocity-component time series used to statistically compare the nested experiments in Fig. 5

5 Nested simulations

5.1 Nesting procedures

Nested experiments are conducted within a rectangular 125×189-point Mercator mesh (Fig. 1) with a horizontal resolution of 0.04° east–west and 0.04° cosϕ north–south, where ϕ is longitude, resulting in a horizontal resolution of ~4 km. For nested regional studies, HYCOM is equipped with open-ocean dynamical boundary conditions for which no distinction is made between inflow and outflow boundaries. The method of characteristics (Browning and Kreiss 1982, 1986) is used for the barotropic open boundary condition on velocity and pressure. At the open boundaries, buffer zones are used to relax temperature and salinity along with the baroclinic pressure and velocity fluctuations toward the fields provided by the outer models. The nesting relaxation zone is 11-grid-points wide (Fig. 1), with the relaxation time scales ranging from 0.1 days at the outer boundary to 24 days at the interior edge.

The topography for the nested WFS domain was extracted directly from the topography used at the Naval Research Laboratory to run both the GoM-free and GoM-NCODA outer models. This topography extends to the 2-m

isobath and contains corrections for passages in the Florida Keys. Since the GoM-free and GoM-NCODA nested experiments used the same grid points as the outer models within the WFS domain, horizontal interpolation of outer model fields to the nested model grid was not required. Both ATL-OI and GLB-NCODA were run at half the resolution of the other outer models with their grid points co-located with every other grid points of the high resolution grid. Thus, horizontal interpolation of outer model fields to every other grid point of the nested model was required. In addition, the minimum coastline isobaths of 20 m for ATL-OI and 10 m for GLB-NCODA required the extrapolation of outer model fields to the shallower nested domain grid points. For both ATL-OI and GLB-NCODA, a small number of deep layers with target densities set to represent the densest waters found in the Atlantic and global oceans were discarded since water of these densities do not exist in the GoM.

Nesting fields are available from the outer model once per day. Linear temporal interpolation of these fields must therefore be performed during model runs to execute the boundary conditions at each baroclinic time step. Vertical resolution is an important issue for the nested models because the vertical coordinate strategy for HYCOM in the stratified open ocean, is to limit the thickness of the near-surface fixed p coordinate domain to maximize the ocean volume represented by isopycnic coordinates. This strategy provides poor vertical resolution above the bottom over the middle and outer continental shelf so that the bottom boundary layer cannot be resolved. Before nesting the coastal models, the thickness of the near-surface p coordinate domain is expanded by adding additional layers with light target densities to the outer model fields (Table 2). The nested models are then run with these same vertical coordinates.

5.2 Experimental procedures

The set of four experiments to be analyzed are listed in Table 1. Since we did not control how the outer model runs were conducted, there are several important differences between the nested and outer model runs. The nested models are forced by higher resolution atmospheric fields, specifically fields obtained from a regional coupled ocean-atmosphere simulation performed using the Coupled Ocean-Atmosphere Mesoscale Prediction System (COAMPS; Hodur et al. 2002) with a horizontal resolution of 27 km. The outer models were forced by fields obtained from the 1.0° degree NOGAPS atmospheric model with the exception of GLB-NCODA, which was forced with the 0.5° NOGAPS model. In all nested experiments except GLB-NCODA, the outer model provided 20 vertical layers in the northeastern GoM, while the nested experiments were run with six additional layers to increase the thickness of the

fixed coordinate domain (Table 2). In GLB NCODA, the outer model provided 28 vertical layers in the northeastern GoM, while the nested experiment was run with four additional layers (Table 2). The nested experiments were all run using KPP mixing with bottom boundary layer parameterization, while the outer models were run using either KPP without a bottom boundary layer parameterization or the Goddard Institute for Space Studies (GISS; Canuto et al. 2002) level 2 turbulence closure. The nested experiments were run with the latest HYCOM version that contained numerous improvements over the code used by the outer models, particularly with respect to the older ATL-OI hindcast.

GLB-NCODA differs in another important aspect from the other outer models. It was run using a 200-hPa reference pressure for layer potential density instead of the surface (0 hPa) reference used in earlier hindcasts. This choice improves representation of the vertical structure of the thermohaline overturning circulation. The same 200-hPa reference pressure was used in the GLB-NCODA nested simulation because conversion to a different reference pressure makes it impossible to preserve isopycnic target densities in model layers. Although horizontal pressure gradients over the shelf will be somewhat less accurate, the inability to preserve isopycnic target densities in isopycnic layers when potential density is converted to a new reference value is also problematic. This issue will be a subject of further research.

All nested experiments were initialized with outer model fields at 0000 UTC on 1 January 2004 and run through 31 December 2005. Model time steps are 6 min for the baroclinic mode and 12 s for the barotropic mode. Three-dimensional simulated fields were archived every 3 h as a compromise between disk storage and aliasing of near-inertial variability. To evaluate nested simulations at the locations of the COMPS moorings, model runs were seeded with synthetic instruments that sample model fields at exactly the same locations and depths at which the observations are available, e.g., at 1-m intervals for velocity components and at the surface (model layer 1) for surface temperature. Variables sampled by the synthetic instruments are saved once per hour to match the observations. Prior to analysis, all observed and simulated time series are low-passed using the MATLAB Chebyshev-2 filter with a half-power point of approximately 40 h to focus on synoptic and longer period variability.

6 Sensitivity of velocity to outer model choice

6.1 Surface flow

Two-year mean surface velocity fields (Fig. 3) reveal differences among the four nested simulations. The mean LC path is nearly identical among the three simulations

Table 1 Properties of the four nested experiments

Nested experiment	Horizontal grid type	Ref. pressure (hPa)	Outer model resolution	Outer model minimum depth (m)	Outer model nest	Outer model mixing model
GoM-free	Mercator	0	0.04°	2	CLIM	GISS
GoM-NCODA	Mercator	0	0.04°	2	CLIM	GISS
ATL-OI	Mercator	0	0.08°	20	GDEM3	KPP-No BBL
GLB-NCODA	Mercator	200	0.08°	10	N/A	KPP-No BBL

Outer model nest refers to the product within which the outer model was nested. Outer model nest "CLIM" refers to a model-generated Atlantic Ocean climatology

nested in data-assimilative outer models, with the core of the current flowing southeastward into the domain near 25° N, then turning eastward to follow the same path through the Florida Straits. The mean path in GoM-free differs from the other three as the core of the LC enters the domain near 26° N, turns southward at the SW end of the WFS, then eastward through the Florida Straits. Effects of the different paths are clearly evident in the large velocity differences that exist

between GoM-free and GoM-NCODA (Fig. 3). Although the mean path is very similar among the three simulations nested in data-assimilative outer models, GLB-NCODA differs from the other two in that the surface velocity magnitude in the LC is about 30% smaller, resulting in the large velocity differences that exist between GoM-NCODA and GLB-NCODA (Fig. 3). These differences are not confined to the LC core. Mean flow along the entire WFS outer shelf

Table 2 Layer target densities (sigma units) for the four outer model products and the six nested experiments

| Layer	Outer models GoM-free, GoM-NCODA, ATL-OI	Nested experiments GoM-free, GoM-NCODA, ATL-OI	Outer model GLB-NCODA	Nested experiment GLB-NCODA
1	19.50	13.50	28.10	23.90
2	20.25	14.50	28.90	25.10
3	21.00	15.50	29.70	26.20
4	21.75	16.50	30.50	27.20
5	22.50	17.50	30.95	28.10
6	23.25	18.50	31.50	28.90
7	24.00	19.50	32.05	29.70
8	24.70	20.25	32.60	30.50
9	25.28	21.00	33.15	30.95
10	25.77	21.75	33.70	31.50
11	26.18	22.50	34.25	32.05
12	26.52	23.25	34.75	32.60
13	26.80	24.00	35.15	33.15
14	27.03	24.70	35.50	33.70
15	27.22	25.28	35.80	34.25
16	27.38	25.77	36.04	34.75
17	27.52	26.18	36.20	35.15
18	27.64	26.52	36.38	35.50
19	27.74	26.80	36.52	35.80
20	27.82	27.03	36.62	36.04
21	27.88	27.22	36.70	36.20
22	27.94	27.38	36.77	36.38
23		27.52	36.83	36.52
24		27.64	36.89	36.62
25		27.74	36.97	36.70
26		27.82	37.02	36.77
27		27.88	37.06	36.83
28		27.94	37.10	36.89
29				36.97
30				37.02
31				37.06
32				37.10

Note that the outer and nested models have the same target densities except that six layers were added to the top of the experiments nested in a GoM outer model, while four layers were added to the top of the experiment nested in the GLB model
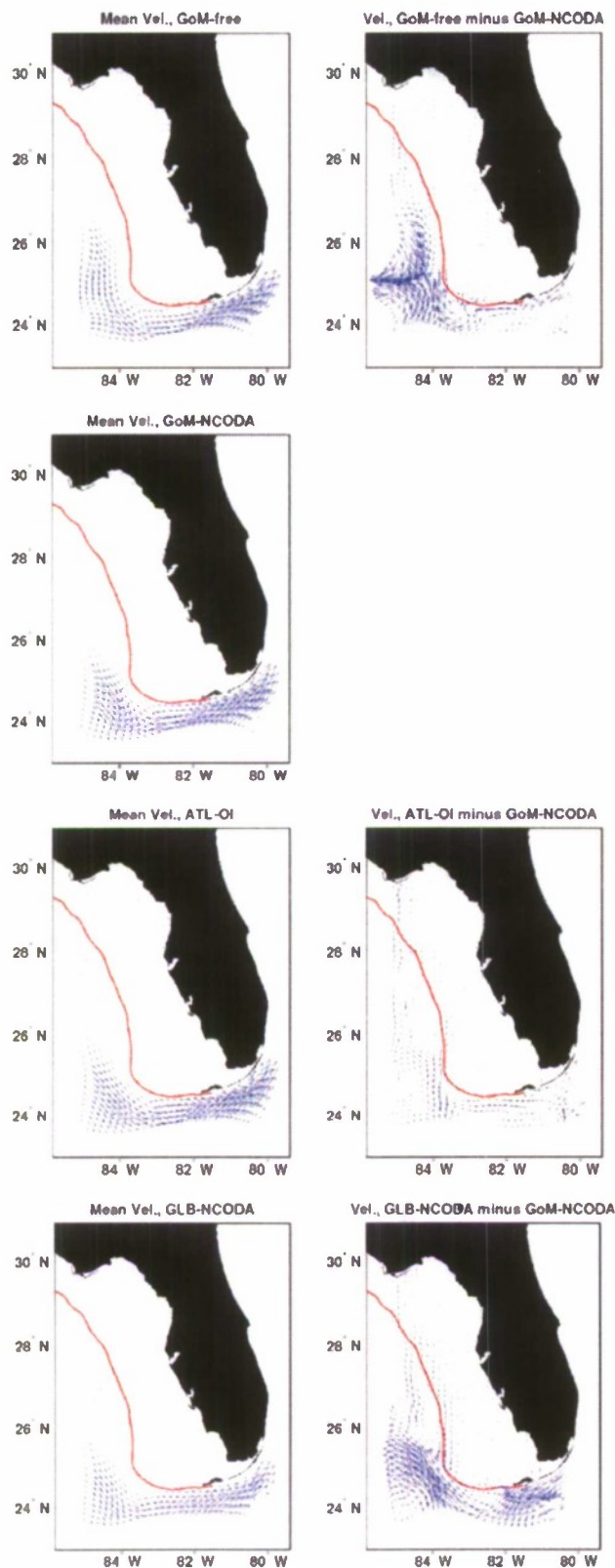
◀ **Fig. 3** Mean surface velocity field over the entire 2004–2005 time interval for, *top to bottom along the left side*, experiments GoM-free, GoM-NCODA, ATL-OI, and GLB-NCODA. The panels from *top to bottom along the right side* show the mean velocity difference between experiments GoM-free, ATL-OI, and GLB-NCODA and experiment GoM-NCODA. The velocity scale for the difference maps has been tripled to more clearly show the difference patterns. The 100-m isobath is shown

and, to a lesser extent, along the entire middle shelf is more northward in GLB-NCODA than in GoM-NCODA. This is the expected flow difference pattern if a weaker LC adjacent to the Dry Tortugas induces weaker southward flow over the outer WFS. Farther offshore, mean flow is more southward in GLB-NCODA than in GoM-NCODA. Thus, the combined contribution of the basin-scale gyre and overturning circulations to LC transport, which is different between GoM-NCODA and GLB-NCODA and incorrectly represented in GoM-NCODA, may have a significant impact on WFS circulation.

The potential importance of LC Dry Tortugas intrusion events is investigated by documenting the strongest event identified in the model simulations, occurring over 14–31 October 2004. Mean velocity fields averaged over this time interval clearly reveal the impact of this event, which is strongest in GoM-NCODA (Fig. 4). In GoM-NCODA, the core of the LC enters the domain between 25° and 26° N and then turns abruptly southward over the continental slope at the SW end of the WFS, providing strong flow immediately adjacent to the shelfbreak. Associated with this pattern is strong southward flow over the outer shelf that extends from the SW end of the WFS (near 25° N) northward to 28° N. Northward flow is also present farther offshore that turns eastward and then southward near 28° N to feed the outer shelf southward flow. This pattern is not present at all in GoM-free because the LC follows a zonal path and does not impinge against the SW end of the WFS. The LC does follow similar paths in the three experiments nested in data-assimilative outer models, but both ATL-OI and GLB-NCODA induce a much weaker southward flow over the outer shelf. The velocity difference map between ATL-OI and GoM-NCODA shows that the southward flow of the LC was slightly farther offshore near 25° N in ATL-OI so that the LC may have been less effective in inducing the southward outer shelf flow. This is also true for GLB-NCODA, although the weaker LC flow in the GLB-NCODA outer model probably contributed to this difference. Unfortunately, this event could not be validated because it occurred at a time when the outer shelf moorings C16 and C18 did not collect observations (Fig. 2).
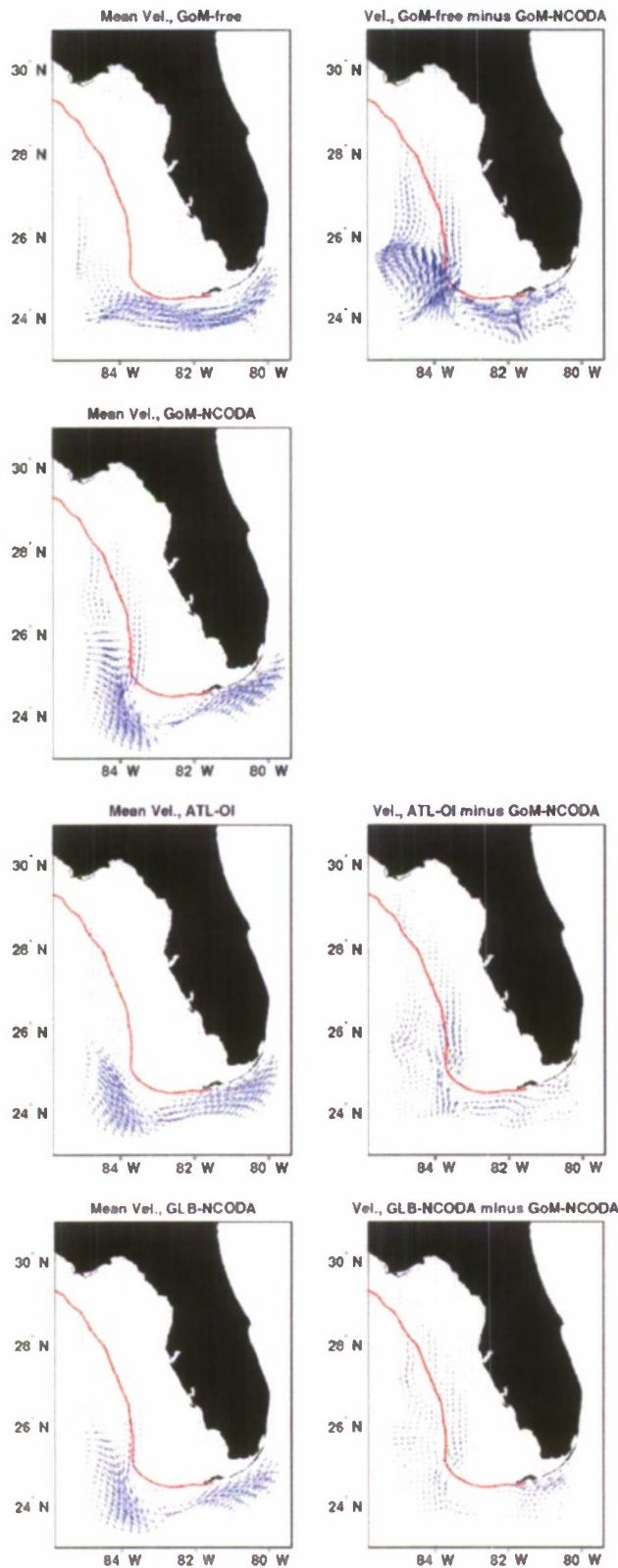
Fig. 4 Same as Fig. 3, but for the time interval 14 to 31 October when a LC intrusion at the SW corner of the WFS apparently drove a strong southward jet over the outer shelf

6.2 ADCP moorings

6.2.1 Inner and middle shelf

Six ADCP moorings are analyzed, which, in order of increasing distance from the coast, are C15, C17, C12, C13, C16, and C18 (Fig. 1). C19 is analyzed in Kourafalou et al. (2008) and is not considered in this study. Vector velocity was rotated so that u and v represents the along- and across-shore components (15° for C12, C15, and C16; 10° for C13; and no rotation for C17 and C18). Taylor (2001) diagrams are used to statistically compare observed and simulated v fluctuations at these moorings at the depths and time intervals marked by the horizontal red lines in Fig. 2. At each mooring, all time series were normalized by the root mean square (RMS) amplitude of the observed time series so that the same Taylor diagram could be used for all six moorings (Fig. 5).

At the two moorings closest to the coast (C15 and C17), little difference exists among the four experiments (Fig. 5). The correlation coefficients range from 0.85 to 0.90 at C15 and are near 0.7 at C17. Given that the normalized RMS amplitude of the observed time series is 1.0, the normalized RMS amplitudes of the four experiments are also very close to 1.0, demonstrating that the simulated v fluctuations have amplitudes very close to the observed value. The RMS differences between the four experiments and observations are all near 0.5. The closeness of these statistics among all four experiments results in closely spaced points on the Taylor diagram (Fig. 5). Similarity among the four experiments is also high at C17, which is located farther from the coast than C15, but the simulations are all less accurate. Correlation coefficients are all close to 0.7. The RMS amplitudes of simulated v are again near 1.0, but the RMS differences between the four experiments and observations are about 0.8. The close statistical similarity among the four experiments at both C15 and C17 (Fig. 5) demonstrates that the choice of outer model has negligible influence on velocity fluctuations over the inner shelf.

At the two mid-shelf moorings C12 and C13, there is more scatter among the four experiments in the Taylor diagrams (Fig. 5). However, this scatter is still relatively small, and the choice of outer model has only a small influence on the quality of the simulations. Correlation coefficients range from 0.5 to 0.7. The RMS amplitudes of simulated v range from 1.1 to 1.3, so the model tends to produce fluctuations that are larger than observed. The RMS differences between the four experiments and observations are all close to 1.0. This decrease of

correlation with distance from the coast is verified in maps of the surface velocity vector correlation coefficient between GoM-NCODA and the other three nested experiments (Fig. 6). Correlation magnitudes between pairs of nested experiments exceed 0.9 over the inner shelf and then decrease steadily over the middle and outer shelf to ~0.5 near the shelfbreak. Velocity variability over the inner shelf is dominated by deterministic wind-driven variability that is nearly identical among the four nested experiments. This

dominance gradually decreases with distance from the coast.

6.2.2 Outer shelf

The scatter among the experiments in the Taylor diagrams (Fig. 5) is largest at outer shelf moorings C16 and C18. At both of these moorings, GLB-NCODA produced v fluctuations that are significantly closer to the observations than

Fig. 5 Taylor diagrams comparing the four nested experiments at six ADCP moorings. The moorings in a through f are arranged in order of increasing distance from the coast. The color legend for the points plotted in each panel is shown at the bottom

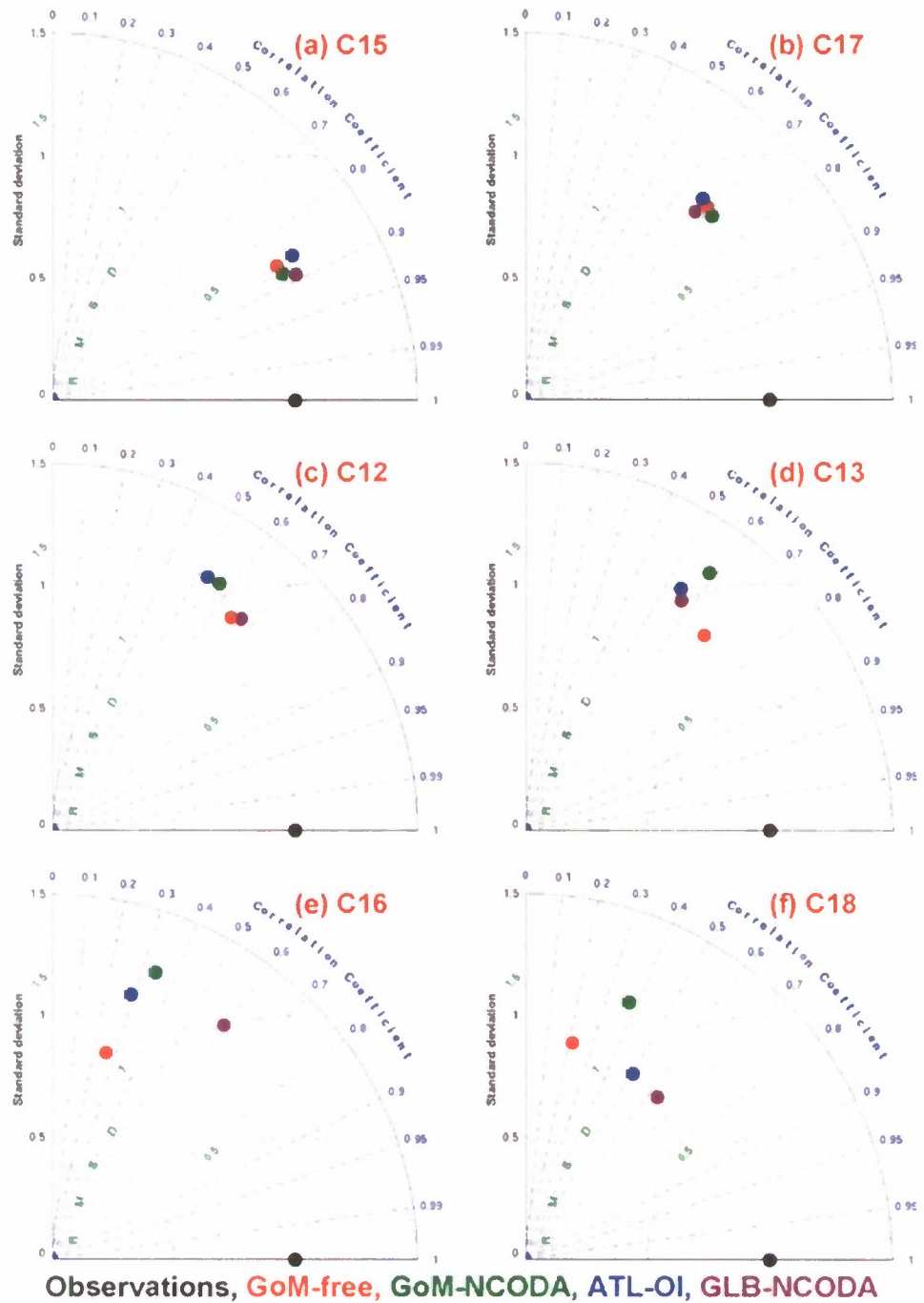Observations, GoM-free, GoM-NCODA, ATL-OI, GLB-NCODA

Fig. 6 Maps of vector correlation magnitude between three-hourly surface velocity fields from nested experiment GoM-NCODA and each of the other three experiments: GoM-free (*left*), ATL-OI (*center*), and GLB-NCODA (*right*). Locations of the six moorings used in the Taylor diagram analysis (Fig. 5) are shown with *black dots*. The three northern moorings are, from offshore to coast, C16, C12, and C15. The three southern moorings are, from offshore to coast, C18, C13, and C17
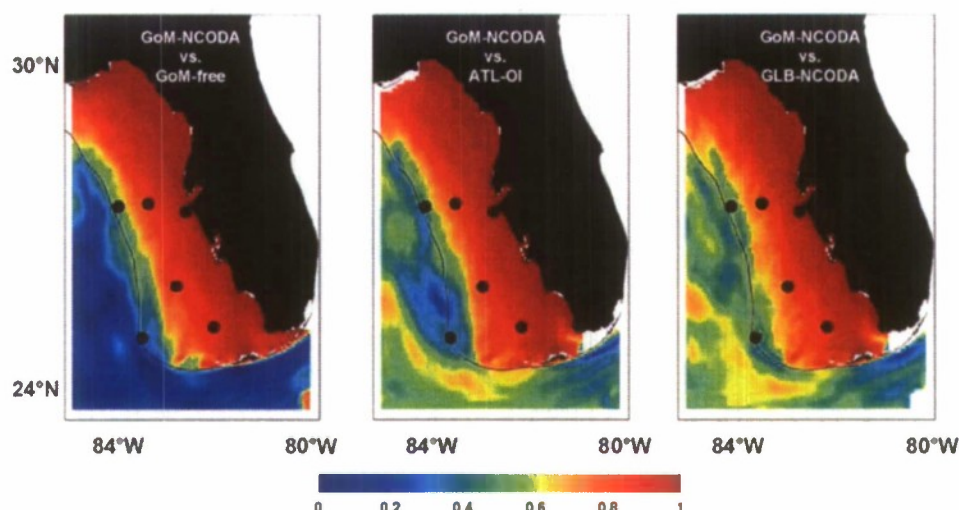
the other nested experiments. The correlation for GLB-NCODA is statistically significant (≈0.6) at both moorings, while the correlations for the other experiments are statistically insignificant. Statistical insignificance is expected between GoM-NCODA and GoM-free because the LC and adjacent eddies are incorrectly represented by the latter experiment. This is illustrated in the surface velocity vector correlation map between these two experiments where correlation magnitude is insignificant everywhere offshore of the shelfbreak (Fig. 6). In contrast, offshore correlation magnitude between GOM-NCODA and both ATL-OI and GLB-NCODA ranges from 0.7 to 0.8 along the LC path between the western boundary and the Dry Tortugas. Although GoM-NCODA and GLB-NCODA use the identical assimilation system, the correlation magnitude fails to exceed 0.8 because the LC transport fluctuations differ substantially between the two outer models. Results from the Taylor diagram analysis suggest that GLB-NCODA provides the most realistic boundary conditions.

Differences among experiments over the outer shelf are further illustrated by time–depth plots of v at C16 from observations and from experiments GoM-free and GLB-NCODA (Fig. 7). Fluctuations in v are dominated by time scales of 1 week to 1 month, and the visual similarity among the fluctuation events between observations and GLB-NCODA is evident. In contrast, fluctuations produced by GoM-free display little resemblance to observations and have a southward mean flow bias relative to both observations and GLB-NCODA.

To further explore why GLB-NCODA is more realistic, two time intervals are analyzed where alongshore flow in the same direction was observed simultaneously at both C16 and C18. During 26 January to 14 February 2005, northward flow is observed simultaneously at both moorings (Fig. 8). A map of surface velocity from GLB-NCODA averaged over this same time interval indicates

that northward flow exists over the outer shelf from 28° N southward to the Dry Tortugas where a cyclonic eddy associated with the LC is producing northward flow along the shelfbreak (Fig. 8). This pattern essentially represents a cyclonic eddy intrusion event at the shelfbreak near the Dry Tortugas that produces alongshore flow along the outer shelf of opposite sign to the classic LC intrusion event. Paluszkiewicz et al. (1983) documented a similar cyclonic eddy intrusion event. During the second time interval (26
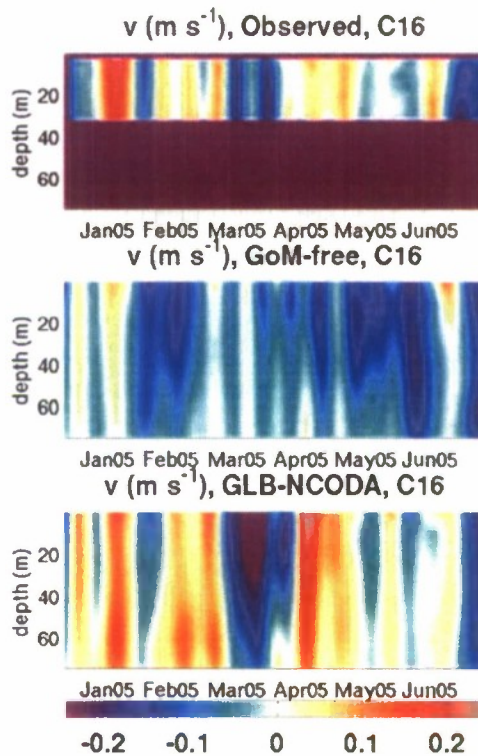

Fig. 7 Time–depth plots of the alongshore velocity component during the first 6 months of 2005 at ADCP mooring C16

Fig. 8 Mean surface velocity maps from experiment GLB-NCODA (*upper left*) over 26 January to 14 February 2005 when persistent northward flow was observed over the outer shelf at both moorings C16 and C18 (*upper right*). Mean surface velocity maps from experiment GLB-NCODA over 26 February 2005 to 17 March 2005 (*lower left*) when southward flow was observed at the same two moorings (*lower right*). The 100-m isobath is shown in the velocity maps
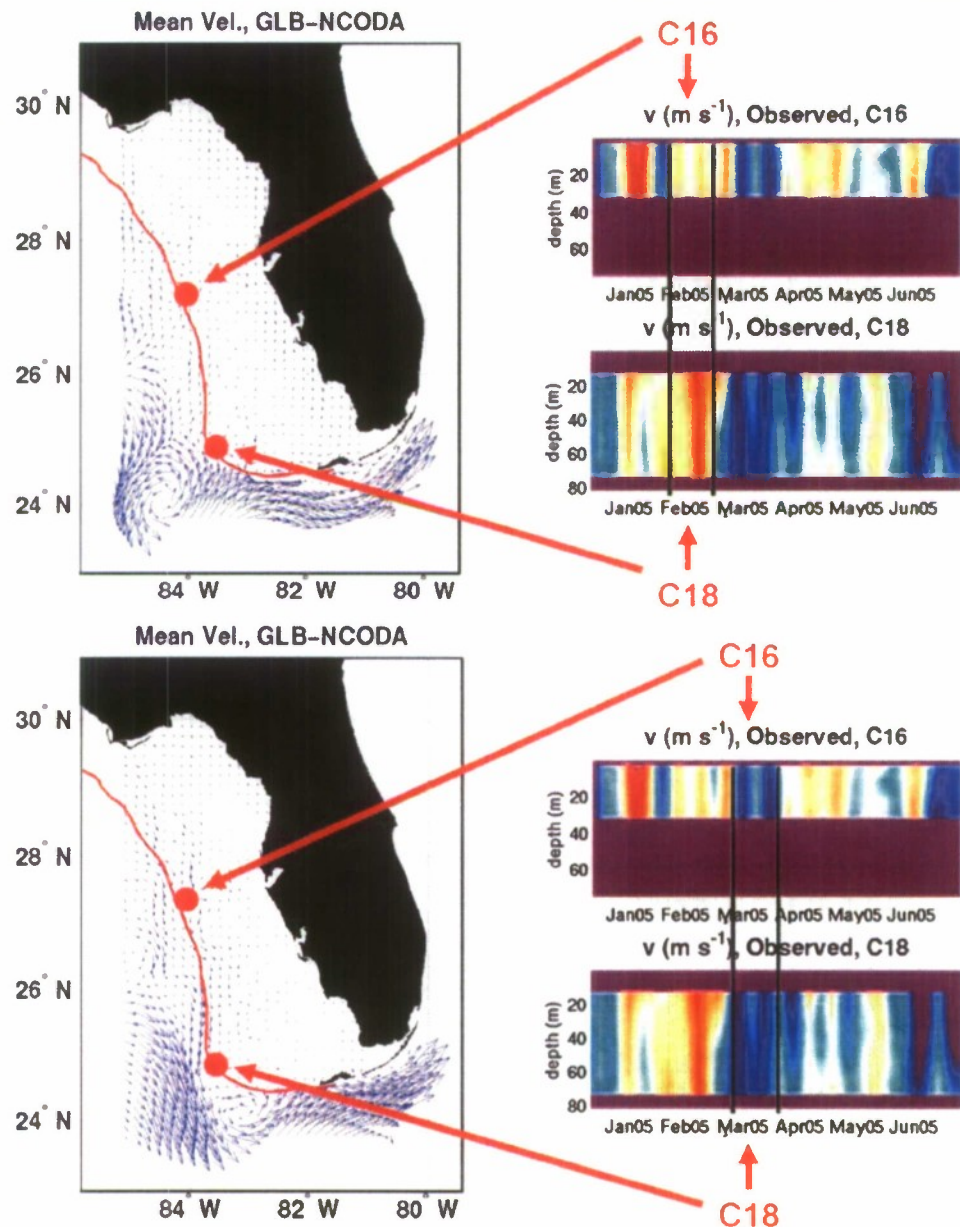
February to 16 March 2005), southward flow is observed at both C16 and C18 (Fig. 8). The mean surface velocity from GLB-NCODA indicates that meandering southward flow exists over the outer shelf along the entire WFS (Fig. 8). By this time, the cyclonic eddy has moved eastward and the LC is situated adjacent to the shelfbreak to produce a classic LC intrusion event.

These outer shelf results are not significantly impacted by the different atmospheric forcing used to drive the outer and nested models. Experiments GoM-NCODA and GLB-NCODA were re-run using the original atmospheric forcing that forced the outer motels, 1.0° NOGAPS for the former and 0.5° NOGAPS for the latter. Maps of surface velocity averaged from 26 February to 16 March for the GLB-

NCODA experiments driven by COAMPS and NOGAPS are compared in Fig. 9. Little difference is observed in the outer shelf and offshore flow patterns, demonstrating insignificant impact from the change in atmospheric forcing. Little difference in mean surface velocity over the outer shelf and slope was also observed for the GoM-NCODA case (not shown).

The boundary conditions not only need to constrain the LC transport and path near the Dry Tortugas to accurately reproduce LC intrusion events but also must constrain the passage of cyclonic eddies that can induce alongshore currents of opposite sign. For this several-week interval during early 2005, the GLB-NCODA boundary conditions successfully constrained the LC and the associated cyclonic
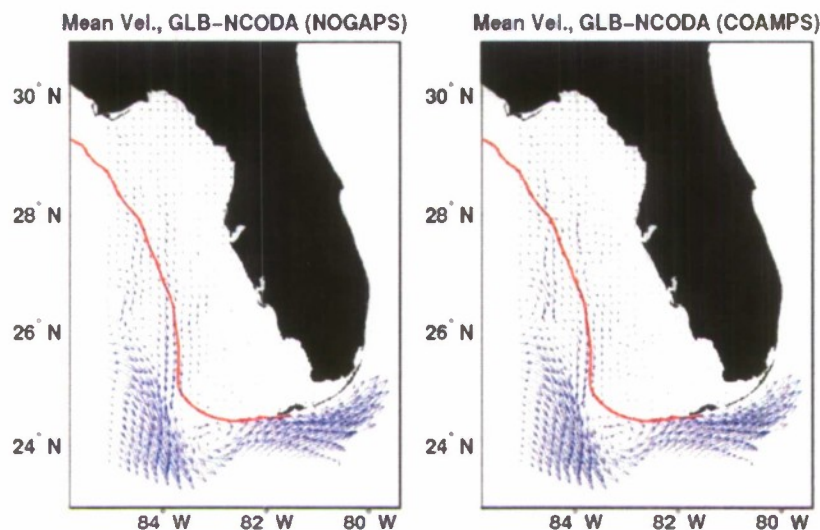
Fig. 9 Mean surface velocity fields over the time interval 26 February 2005 through 17 March 2005 from experiment GoM-NCODA (*left*) and a second GLB-NCODA experiment (*right*) that was forced by atmospheric fields from the same Navy 0.5°-degree NOGAPS atmospheric model that was used to force the GLB-NCODA outer model. The 100-m isobath is shown

eddy to reproduce the alongshore flow reversals that actually occurred over the WFS. Cyclonic eddies such as the one considered in this study continue on to form the so-called Tortugas Gyres that significantly impact circulation in the Florida Straits south of the Florida Keys. The impact of these events, including this particular cyclonic eddy, on circulation in the Florida Straits is studied further in Kourafalou et al. (2008).

7 Sensitivity of temperature to outer model choice

Sea surface temperature time series available from surface instruments on some of the ADCP moorings are examined to determine to what extent they are sensitive to the different boundary conditions and to determine if improvements can be realized by nesting in data-assimilative ocean hindcasts (Fig. 10). As for the ADCP observations, the temperature time series have gaps limiting time intervals that can be analyzed.

Relatively long time series with minimal gaps are available simultaneously at the two inner-shelf moorings C10 and C14 from December 2004 through December 2005 (Fig. 10a, b). All experiments reproduce the annual cycle of surface temperature variability with reasonable fidelity. Relatively small differences are expected because surface temperature is expected to approximately track air temperature given that bulk formula are used to calculate surface turbulent heat flux during model runs and because the same atmospheric forcing fields drive all of the experiments. Differences among the models are very small from late spring through mid-autumn as expected. However, differences become substantially larger (1–2°C) during

the cold season when strong atmospheric-forcing events mix deeper water up to the surface and weaken the surface temperature constraint imposed by the atmospheric forcing. The offshore boundary conditions apparently do exert a significant influence on temperature at inner shelf stations, although it is only detected at the surface when vertical mixing is strong. Thermal differences imposed at the outer boundary will influence the temperature of offshore waters that are exchanged with shelf waters across the shelfbreak. The interplay of flow variability over the shelf due to both atmospheric and offshore forcing can then transmit these temperature anomalies throughout the WFS, with the frictional bottom boundary layer likely playing an important role in cross-shelf transport (Weisberg et al. 2005).

Farther offshore, time series at moorings C12, C13, and C17 for mid-September through early December 2005 demonstrate that the model reproduces the fall cooling with reasonable fidelity (Fig. 10c–e). Temperature at C12 and C13 are >1°C too cold during the first half of the time interval but are in better agreement with observations after hurricane Wilma passed in late October. Model temperatures are in good agreement with one distinct exception: Temperatures produced by the GoM-free experiment become too cold after the first of November. Temperature time series are also presented for two winter time intervals, at C12 during winter 2004 (Fig. 10f) and at C17 during winter 2005 (Fig. 10g). Although the models reproduce synoptic fluctuations with reasonable fidelity, the relatively large winter differences among the nested experiments are clearly evident. Also evident again is the tendency for the GoM-free experiment to produce temperatures that are too cold.

The cold SST bias produced by GoM-free during the cold season at mid-shelf moorings is explored further by
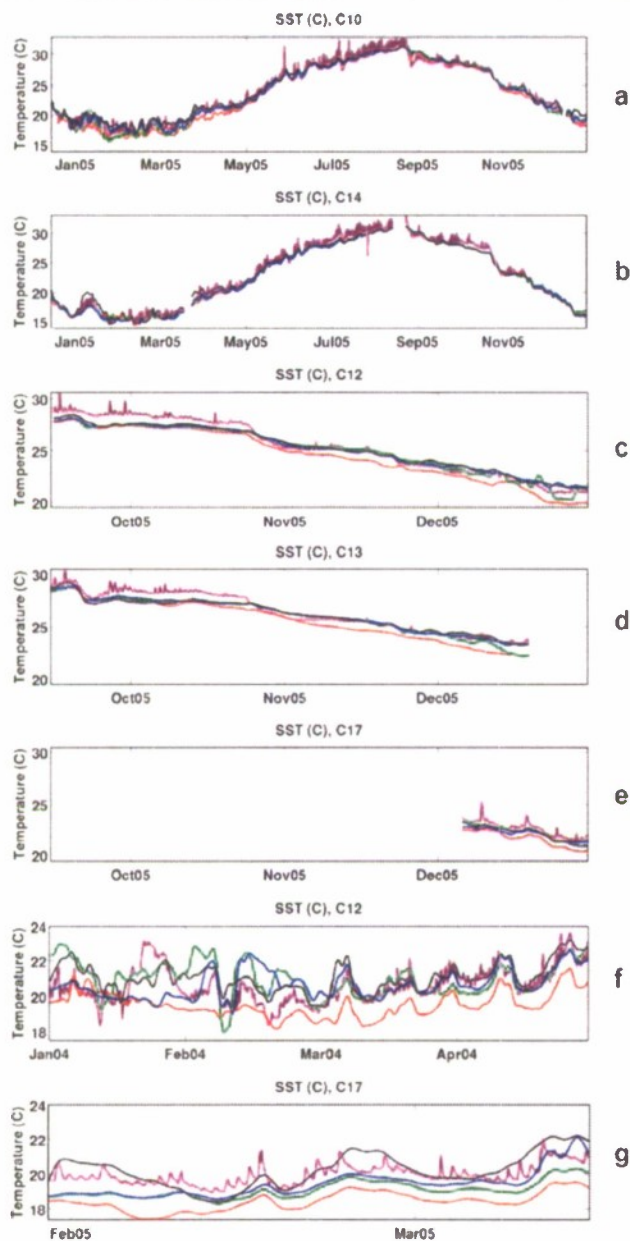
Fig. 10 Sea surface temperature time series for selected time intervals measured by surface instrumentation at the COMPS moorings. Subpanels **a** and **b** are for nearshore moorings C10 and C14 for mid-December 2004 through 2005. Subpanels **c**, **d**, and **e** are for moorings C12, C13, and C17 during fall 2005. Subpanels (**f**) and (**g**) are for two winter/spring intervals, C12 for 2004 and C17 for 2005. *Red lines* are for experiment GoM-free, *green lines* for GoM-NCODA, *blue lines* for ATL-OI, and *solid black lines* for GLB-NCODA. The *magenta lines* represent the observations

analyzing simulated temperature variability as a function of depth and time at mid-shelf mooring C12 (Fig. 11). The depth–time plot for temperature from experiment GoM-NCODA clearly reveals the two seasonal cycles along with abrupt mixing events during late summer and fall of both

years due to frequent hurricane passage. The other three panels in Fig. 11 show the temperature difference between the other three experiments and GoM-NCODA. Experiment GoM-free tends to be substantially colder than the other three experiments. The source of this problem is that the non-assimilative GoM-free outer model has a persistent cold bias in the upper ocean that was substantially corrected by the data assimilation used in the other outer models (not shown). Experiment GoM-free was therefore initialized with fields that had a cold bias, and the boundary conditions maintained this cold bias relative to the other experiments throughout the two year run. Given that GoM-free produces isotherms near the shelfbreak that are higher in the water column than the other experiments, water exchanges across the shelfbreak will lead to colder water moving onto the WFS. Weisberg et al. (2005) discusses scenarios where the interplay of atmospheric and offshore forcing can transmit offshore water with abnormal properties over most of the WFS, even well onto the inner shelf. It is therefore important that the chosen outer model have a reasonably accurate upper ocean temperature structure. The
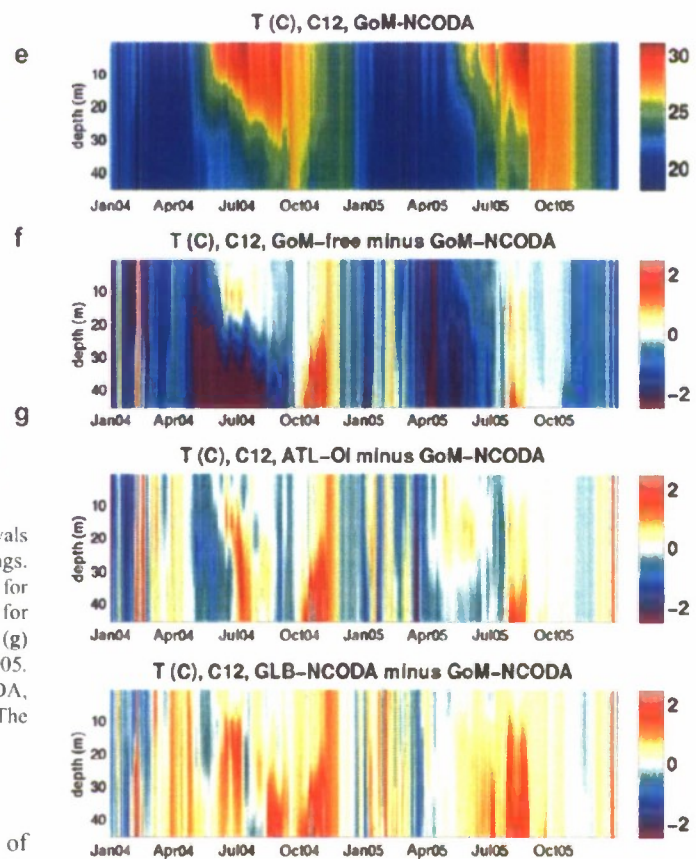

Fig. 11 Depth–time plot of temperature at mooring C12 simulated by experiment GoM-NCODA (*top panel*) along with the temperature differences observed between experiments GoM-free, ATL-OI, and GLB-NCODA and experiment GoM-NCODA (*bottom three panels*)
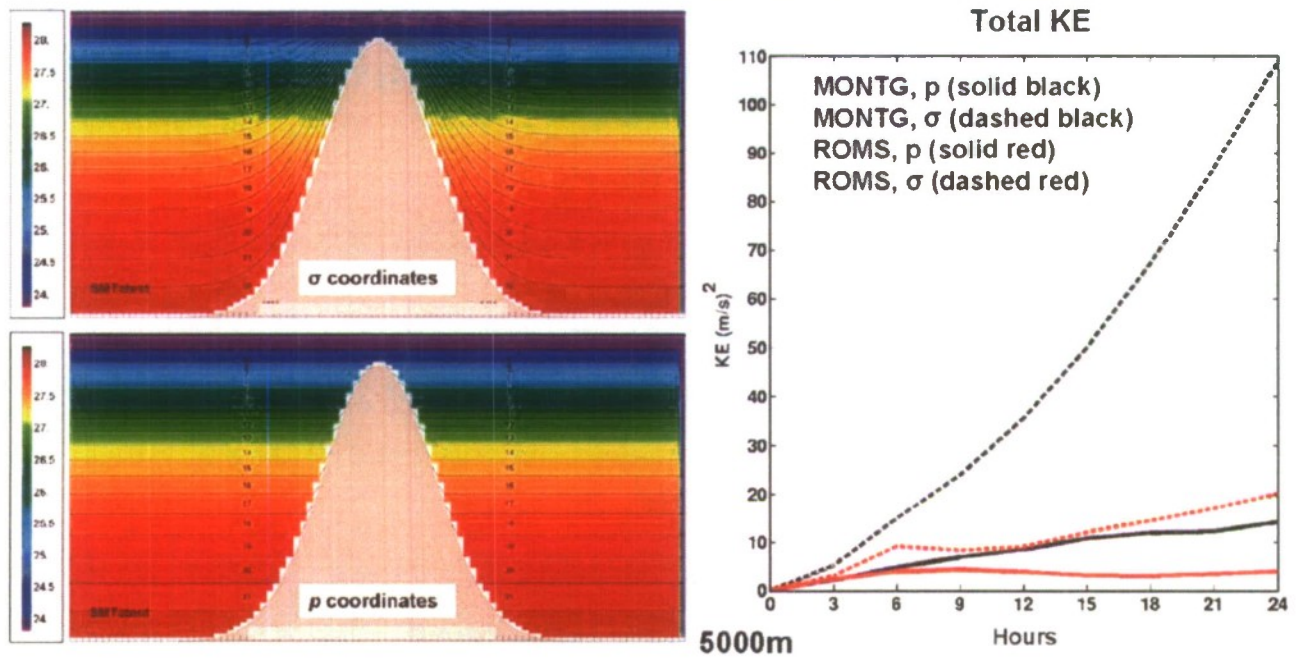
Fig. 12 Initial density field and vertical coordinates for the p and σ coordinate seamount tests (*left*). Temporal evolution of kinetic energy over the first day of integration for the four seamount tests

present results document the advantages of nesting within outer models where data assimilation has improved the upper-ocean structure of temperature (and presumably other water properties).

8 Conclusions

We achieved limited success in detecting positive impacts of nesting a coastal ocean model of the WFS within data assimilative ocean hindcasts during 2004–2005. Concerning flow variability over the WFS, the ability of the outer model to accurately constrain both the path and flow velocity of the LC and associated eddies off the southwestern end of the WFS had a positive impact on the simulation of alongshore flow along the outer WFS. Experiment GoM-free nested in a non-assimilative outer model did not reproduce alongshore flow events that were observed at two outer shelf ADCP moorings, while experiment GLB-NCODA reproduced them most realistically. Although GoM-NCODA used the same observations and assimilation system as GLB-NCODA, the former was a regional model nested in Atlantic basin climatology that did not contain realistic LC transport variability associated with the wind-driven gyre circulation and the Atlantic Meridional Overturning Circulation. This absence of realistic transport variability is one possible reason why the GoM-NCODA nested simulation produced less realistic outer shelf flow variability than GLB-NCODA. Since the impact of offshore flow variability tends to be confined to the outer

shelf due to the Taylor–Proudman constraint and since deterministic wind-driven flow variability gradually becomes dominant toward the coast, the choice of outer model did not significantly influence flow variability over the middle and inner shelf.

Another positive impact was observed in the representation of temperature over the WFS. The non-assimilative outer model GoM-free had a significant cold bias in the upper ocean relative to the three data-assimilative outer models. This cold bias was presumably communicated across the WFS during the 2-year experiments because the existence of surface and bottom Ekman layers breaks the Taylor–Proudman constraint and permits efficient cross-shelf exchanges of water properties. The cold bias was nearly always present below the surface mixed layer during the 2004–2005 time interval but was only detectable in moored surface temperature measurements during the cold season when strong atmospheric forcing mixed the cold water up to the surface. It is very important for the outer model to accurately represent the upper-ocean temperature (along with salinity and density) structure so that offshore water with the correct properties is entrained onto the WFS.

The present analysis also contributed to the ongoing development of HYCOM as a coastal ocean model. In particular, it was demonstrated that the use of level p coordinates over the continental shelf and shelfbreak region instead of σ coordinates can reduce pressure gradient errors (Appendix) and does not require special numerical techniques to represent sloping topography that are necessary for Eulerian Vertical Dynamics models such as MOM.

Although we are encouraged by the ability to detect positive impacts of nesting in data-assimilative outer models, the results presented in this paper are based on limited space–time observational coverage. This is particularly true for the velocity measurements available along the outer shelf. Further study is necessary to accurately quantify the importance of the intrusion of the LC and associated cyclones at the shelfbreak and near the Dry Tortugas. It is clear from the present analysis that accurate representation of the LC path and transport by the chosen outer model is critically important to achieve this goal.

Appendix: Vertical coordinate selection

The first application of HYCOM as a coastal model (Winther and Evensen 2006) demonstrated that the model could produce realistic circulation and water mass structure in shallow water regions. They used the standard approach for coastal regions of allowing the offshore isopycnic and nearsurface level p coordinates to transition to σ coordinates over shallow water. The classic seamount problem (e.g., Beckmann and Haidvogel 1993) is used in this study to demonstrate the superiority of using p instead of σ coordinates in coastal regions with sloping topography.

The seamount domain was set up in a 360×360-km f-plane box, with f set to its value at $30°$ N, and uses the seamount structure of Shchepetkin and McWilliams (2003):

$$h(x, y) = H_0 - H \exp\left(\frac{-(x^2 + y^2)}{L^2}\right)$$

where $L = 5{,}000$ m, $H = 4{,}500$ m, and $L = 40$ km. The continuous initial density profile is exponential and roughly representative of summer density profiles observed in the subtropical Atlantic. The Burger number is ~3, an intermediate value in the range of cases considered in earlier seamount tests (e.g., Beckmann and Haidvogel 1993; Mellor et al. 1998; Shchepetkin and McWilliams 2003). Twenty-two vertical layers were used for both the p and σ coordinate cases. To initialize model fields, the density value of each layer was first assigned as a function of central layer depth based on the initial continuous density profile. To assign initial T and S values to each layer, an exponential

temperature profile roughly representative of the summer subtropical Atlantic was used to assign T values at central layer depths; then, S values were calculated using the model equation of state. Initial cross-sections of density for both vertical coordinate choices are presented in Fig. 12. In addition to the two cases run with the existing Montgomery potential formulation of the pressure gradient force (MP), two additional cases were run implementing the pressure gradient formulation used in the ROMS ocean model (Shchepetkin and McWilliams 2003).

For each of the four cases, the model was run unforced for 24 h. The resulting currents resulted from errors in the pressure gradient force, and the effects of these errors were monitored by graphing the total kinetic energy as a function of time (Fig. 12). The most rapid increase in KE occurs for the σ coordinate, MP case. The rate of increase was much smaller for the p coordinate, MP case because pressure gradient errors at any grid point are confined to the deepest layer with non-zero thickness that intersects a sloping bottom while errors exist in shallower σ coordinate layers. A similar scenario is observed for the two ROMS cases, with the smallest rate of KE increase occurring in the p coordinate case. These results demonstrate the superiority of using p coordinates over sloping topography in HYCOM. Ideally, the ROMS pressure gradient formulation should also be used, but there is a significant problem in the interior isopycnic coordinate domain. If a level isopycnic layer intersects a sloping bottom, there should be zero pressure gradient force, and this is achieved with high accuracy by the MP formulation. However, this situation produces adjacent grid points where the sloping bottom is shallower than the level interface at the bottom of the layer, resulting in a change of central layer depth between the grid points. Given the constant density in this layer, the ROMS formulation detects a sloping density interface and produces a non-zero pressure gradient force where none should exist. Tests demonstrated that this problem more than nullified the improvements produced by the ROMS formulation in the non-isopycnic coordinate domain (not shown). Therefore, the MP formulation was retained and p coordinates used for the nested coastal simulations in this study. This is a reasonable choice because the rate of KE increase in the seamount tests was comparable to the rate of increase for the ROMS formulation used with σ coordinates (Fig. 12).

References

Adcroft A, Hallberg R (2005) On methods for solving the oceanic equations of motion in generalized vertical coordinates. Ocean Model 11:224–233

Adcroft A, Hill C, Marshall J (1997) Representation of topography by shaved cells in a height coordinate ocean model. Mon Weather Rev 125:2293–2315

Barth A, Alvera-Azcárate A, Weisberg RH (2008) Benefit of nesting a regional model into a large-scale ocean model instead of climatology. Application to the West Florida Shelf. Cont Shelf Res 28:561–573, doi:10.1016/j.csr.2007.11.004

Beckmann A, Haidvogel DB (1993) Numerical simulation of flow around a tall isolated seamount, 1, problem formulation and model accuracy. J Phys Oceanogr 23:1736–1753

Bleck R (1998) Ocean modeling in isopycnic coordinates. In: Chassignet EP, Verron J (eds) Ocean modeling and parameterization, Chapter 18. NATO Sci Ser Gen Sub-ser C Math Phys Ser 516:423–448

Bleck R (2002) An oceanic general circulation framed in hybrid isopycnic-Cartesian coordinates. Ocean Model 4:55–88

Bleck R, Rooth C, Hu D, Smith LT (1992) Ventilation patterns and mode water formation in a wind- and thermodynamically driven isopycnic coordinate model of the North Atlantic. J Phys Oceanogr 22:1486–1505

Browning GL, Kreiss H-O (1982) Initialization of the shallow water equations with open boundaries by the bounded derivative method. Tellus 34:334–351

Browning GL, Kreiss H-O (1986) Scaling and computation of smooth atmospheric motions. Tellus 38A:295–313

Canuto VM, Howard A, Cheng Y, Duhovikov MS (2002) Ocean turbulence. Part II: vertical diffusivities of momentum, heat, salt, mass, and passive scalars. J Phys Oceanogr 32:240–264

Chapman DC, Brink KH (1987) Shelf and slope circulation induced by fluctuating offshore forcing. J Geophys Res 92:11741–11759

Chassignet EP, Smith L, Halliwell GR, Bleck R (2003) North Atlantic simulation with the hybrid coordinate ocean model (HYCOM): impact of the vertical coordinate choice and resolution, reference density, and thermobaricity. J Phys Oceanogr 33:2504–2526

Chassignet EP, Hurlburt HE, Smedstad OM, Halliwell GR, Hogan PJ, Wallcraft AJ, Bleck R (2006) Ocean prediction with the Hybrid Coordinate Ocean Model (HYCOM). In: Chassignet EP, Verron J (eds) Ocean weather forecasting: an integrated view of oceanography. Springer, Berlin, pp 413–426

Chassignet EP, Hurlburt HE, Smedstad OM, Halliwell GR, Hogan PJ, Wallcraft AJ, Bleck R (2007) Ocean Prediction with the HYbrid Coordinate Ocean Model (HYCOM). J Mar Syst 65:60–83

Cooper M, Haines K (1996) Altimetric assimilation with water property conservation. J Geophys Res 101:1059–1078

Cragg J, Mitchum G, Sturges W (1983) Wind-induced sea surface slopes on the West Florida Shelf. J Phys Oceanogr 13:2201–2212

Cummings JA (2005) Operational multivariate ocean data assimilation. Q J R Meteorol Soc 131:3583–3604

Fox DN, Teague WJ, Barron CN, Carnes MR, Lee CM (2002) The Modular Ocean Data Analysis System (MODAS). J Atmos Ocean Technol 19:240–252

Halliwell GR Jr (2004) Evaluation of vertical coordinate and vertical mixing algorithms in the hybrid-coordinate ocean model (HYCOM). Ocean Model 7:285–322

Halliwell GR Jr, Shay LK, Jacob SD, Smedstad OM, Uhlhorn EW (2008) Improving ocean model initialization for coupled tropical cyclone forecast models using GODAE nowcasts. Mon Weather Rev 136:2576–2591

He R, Weisberg RH (2002) Tides on the West Florida Shelf. J Phys Oceanogr 32:3455–3473

He R, Weisberg RH (2003) A loop current intrusion case study on the West Florida Shelf. J Phys Oceanogr 33:465–477

Hetland RD, Hsueh Y, Leben RR, Niiler PP (1999) A loop current-induced jet along the edge of the West Florida Shelf. Geophys Res Lett 26:2239–2242

Hodur RM, Pullen J, Cummings J, Hong X, Doyle D, Martin PJ, Rennick MA (2002) The Coupled Ocean/Atmospheric Mesoscale Prediction System (COAMPS). Oceanography 15:88–98

Huh OK, Wiseman WJ, Vansant LL (1981) Intrusion of loop current waters onto the west Florida continental shelf. J Geophys Res 86:4186–4192

International GODAE Steering Team (2000) Global ocean data assimilation experiment strategic plan. GODAE Report #6, GODAE International Project Office, Bureau of Meteorology, Melbourne, Australia (26 pp)

Jacobs GA, Barron CN, Rhodes RC (2001) Mesoscale characteristics. J Geophys Res 106:19,581–19,595

Kelly KA, Chapman DC (1988) The response of stratified shelf and slope waters to steady offshore forcing. J Phys Oceanogr 18:906–925

Kourafalou VH, Peng G, Kang H, Hogan PJ, Smedstadt OM, Weisberg RH, Baringer MO, Meinen CS (2008) Evaluation of global ocean data assimilation experiment products on South Florida nested simulations with the Hybrid Coordinate Ocean Model. Ocean Dynamics (this issue)

Large WG, Mc Williams JC, Doney SC (1994) Oceanic vertical mixing: a review and a model with a nonlocal boundary layer parameterization. Rev Geophys 32:363–403

Liu Y, Weisberg RH (2005) Patterns of ocean current variability on the West Florida Shelf using the self-organized map. J Geophys Res 110:C06003, doi:10,1029/2004JC002786

Liu Y, Weisberg RH (2007) Ocean currents and sea surface heights estimated across the West Florida Shelf. J Phys Oceanogr 37:1697–1713

Marmorino GO (1983) Variability of currents, temperature, and bottom pressure across the West Florida continental shelf, winter 1981–1982. J Geophys Res 88:4439–4457

Mellor GL, Oey L-Y, Ezer T (1998) Sigma coordinate pressure gradient errors and the seamount problem. J Atmos Ocean Technol 15:1122–1131

Mitchum TG, Clarke AJ (1986a) The frictional nearshore response to forcing by synoptic scale winds. J Phys Oceanogr 16:934–946

Mitchum TG, Clarke AJ (1986b) Evaluation of frictional, wind forced long wave theory on the West Florida Shelf. J Phys Oceanogr 16:1029–1037

Mitchum TG, Sturges W (1982) Wind-driven currents on the West Florida Shelf. J Phys Oceanogr 12:1310–1317

Niiler PP (1976) Observations of low-frequency currents on the West Florida continental shelf. Mem Soc Roy Sci Leige 6:331–358

Paluszkiewicz T, Atkinson L, Parmentier ES, McClain CS (1983) Observations of a loop current frontal eddy intrusion onto the West Florida Shelf. J Geophys Res 88:9639–9651

Shchepetkin AF, McWilliams JC (2003) A method for computing pressure-gradient force in an oceanic model with a non-aligned vertical coordinate. J Geophys Res 108:3090, doi:10.1029/2001JC001047

Taylor KE (2001) Summarizing multiple aspects of model performance in a single diagram. J Geophys Res 106:7183–7192

Weisberg RH, He R (2003) Local and deep-ocean forcing contributions to anomalous water properties on the West Florida shelf. J Geophys Res 108(C6):15, doi:10.1029/2002JC001407

Weisberg RH, Black BD, Li Z (2000) An upwelling case study on Florida's west coast. J Geophys Res 105:11,459–11,469

Weisberg RH, Li Z, Muller-Karger F (2001) West Florida shelf response to local wind forcing: April 1998. J Geophys Res 106:31239–31262

Weisberg RH, He R, Kirkpatrick G, Muller-Karger F, Walsh JJ (2004) Coastal ocean circulation influences on remotely sensed optical properties: a West Florida Shelf case study. Oceanography 17:68–75

Weisberg RH, He R, Liu Y, Virmani JI (2005) West Florida Shelf circulation on synoptic, seasonal, and interannual time scales. In: Circulation in the Gulf of Mexico: observations and models. Geophys Monogr 161:325–347

Winther NG, Evensen G (2006) A hybrid coordinate ocean model for shelf sea simulation. Ocean Model 13:221–237